High-temperature annealing of ($\bar{2}$01) β-Ga$_2$O$_3$ substrates for reducing structural defects after diamond sawing

Pavel Butenko[1, †], Michael Boiko[2], Mikhail Sharkov[2], Aleksei Almaev[3], Aleksnder Kitsay[2], Vladimir Krymov[2], Anton Zarichny[3], and Vladimir Nikolaev[1, 2]

[1]MISiS University, Moscow 119049, Russia

[2]Perfect Crystala LLC, St. Petersburg 194223, Russia

[3]Tomsk State University, Tomsk 634050, Russia

Abstract: A commercial epi-ready ($\bar{2}$01) β-Ga$_2$O$_3$ wafer was investigated upon diamond sawing into pieces measuring 2.5 × 3 mm^2. The defect structure and crystallinity in the cut samples has been studied by X-ray diffraction and a selective wet etching technique. The density of defects was estimated from the average value of etch pits calculated, including near-edge regions, and was obtained close to 10^9 cm^{-2}. Blocks with lattice orientation deviated by angles of 1−3 arcmin, as well as non-stoichiometric fractions with a relative strain about $(1.0-1.5) \times 10^{-4}$ in the [$\bar{2}$01] direction, were found. Crystal perfection was shown to decrease significantly towards the cutting lines of the samples. To reduce the number of structural defects and increase the crystal perfection of the samples via increasing defect motion mobility, the thermal annealing was employed. Polygonization and formation of a mosaic structure coupled with dislocation wall appearance upon 3 h of annealing at 1100 °C was observed. The fractions characterized by non-stoichiometry phases and the block deviation disappeared. The annealing for 11 h improved the homogeneity and perfection in the crystals. The average density of the etch pits dropped down significantly to 8×10^6 cm^{-2}.

Key words: gallium oxide; epi-ready substrate; etch pits; crystal defect; mosaic structure; crystal perfection

1. Introduction

Ga$_2$O$_3$ is a novel ultra-wide band gap (UWBG) semiconductor that has attracted the attention of many researchers over the previous decade. This material is a promising one for microelectronics, especially in a bulk form[1]. In particular, it is already used as semi-insulating substrates prepared for epitaxy processes (so-called "epi-ready substrates")[2]. Among all known gallium oxide polymorphs (α-, β-, δ-, γ-, $\varepsilon(\kappa)$-), the β-one is the only modification that can be grown from the melt at the normal pressure as a bulk single crystal[1, 2].

The most common technique of liquid-phase β-Ga$_2$O$_3$ bulk single-crystal growth is the edge-defined film-fed growth (EFG)[1, 2]. It is applied in manufacturing high-quality crystals of a given shape. The grown wafers are then chopped or cut into pieces for substrates production. Finally, to obtain epi-ready substrates that allow one to perform successful epitaxial processes, the β-Ga$_2$O$_3$ samples are subjected to post-growth processing. The latter one consists of the following stages: cutting, grinding, polishing and chemical−mechanical polishing (CMP). It is known that mechanical treatment of crystals generate the structural defects in their subsurface layer[3, 4]. It was shown that on cutting the gallium oxide bulk crystal into slices (a slicing procedure) and subsequent grinding, the subsurface layers contain extended tongue-patterned cleavage pits[5]. Microcracks located under

such pits, which the authors attribute to the presence of cleavage planes in β-Ga$_2$O$_3$. In spite of the fact that, at the final post-growth processing stage (which is a CMP), tongue-like pits were eliminated and a low surface roughness (R_a = 0.18 nm) was achieved, the authors failed to get rid of the microcrack propagation deep into the sample. Other researchers confirmed that it is impossible to eliminate a significant portion of defects generated into (001) β-Ga$_2$O$_3$ wafers during cutting even after CMP[6]. The paradoxical situation that arose during the study of the Schottky barrier diode (SBD) characteristics based on β-Ga$_2$O$_3$ is of interest[7]. It has been noted that most surface inhomogeneities, in the form of etch pits actually produced unintentionally, appear as a result of the CMP.

This brief list of the publications devoted to mechanical treatment of gallium oxide wafers shows that the problem of defect formation during the post-growth treatment of β-Ga$_2$O$_3$ substrates exists. Therefore, this issue requires study, especially in the case of epi-ready substrate production, where the problem is completely applicable.

In this paper a commercial epi-ready ($\bar{2}$01) β-Ga$_2$O$_3$ wafer was subjected to being cut into pieces. The edge regions of the samples were studied in order to reveal the defects of their structure and a degree of crystal perfection. Further annealing was applied to activate the defect mobility and improve the sample structure.

2. Materials and methods

A commercial single-crystal ($\bar{2}$01) β-Ga$_2$O$_3$ 2-inch double-sided CMP wafer was studied. According to the specification,

---

the unintentionally doped (UID) epi-ready wafer has a diameter of 50.8 ± 0.3 mm and a thickness of 680 ± 20 μm. The crystal perfection given via FWHM (full width at half maximum) of XRD (X-ray diffraction) ω-scan were 22.3 and 15.8 arcsec for 020 and 204 reflections, correspondingly. The wafer was glued on the textolite plate and cut into rectangular samples (2.5×3 mm^2) with a precision diamond disk saw. The inner-type cutting wheel thickness was 0.20 mm and the wheel grain size was 60×40 μm. The cutting line speed (saw motion relative to the sample) was 0.5 mm/min and the wheel rotation speed was 3000 r/min. Afterward, the samples were detached from the textolite plate and washed in ethanol and distilled water. The ($\bar{2}$01) plane surface of these "as-cut" samples participated in the experiments.

The surfaces of the samples were examined by the MarSurf PS-10 profilometer in order to determine their roughness. XRD measurements were performed at a modified Bourevestnik DRON-7 setup with Cu K$_{\alpha 1}$ (1.5406 Å) irradiation and a Ge (111) monochromator crystal in the two-crystal mode. Signal registration was implemented using a scintillation SCSD-4C detector in the reflection Bragg mode. A set of reflection curves in both θ–2θ and ω-modes were recorded for the samples around the $\bar{2}$01 reflection and the fold ones. Applying the ω-scanning mode makes it possible to obtain an estimation of the block mismatch angle. With its help, one can observe the changes in the dynamics of the lattice parameters in individual areas of the β-Ga$_2$O$_3$ samples.

It should be specified, that conventional XRD signals from powder samples contain peaks that describe different reflections being a characteristic of the sample lattice. However, XRD datasets collected at single crystals and mosaic samples consisting of coherent/quasi-coherent domains look different than powder XRD curves. In the case of mosaics, they usually yield only a set of XRD reflections corresponding to a certain wave vector direction (in most cases, the normal to the sample surface).

The Williamson−Hall model[8] for processing a set of reflections was applied to the obtained θ–2θ XRD curves. The FWHM values of reflection curves (denoted as W_{II}) are known to be defined by two dominating factors (crystallite sizes and micro-stresses) described by Gauss functions, which fit the registered curve on being convoluted. The W_{II} value can be expressed as follows:

$$W_{\mathrm{II}}^2 = \left(\frac{\lambda}{t_z}\right)^2 + \left((4\langle\varepsilon\rangle)^2 + \left(\frac{\lambda}{t_z}\right)^2\right)\tan^2\theta_{\mathrm{b}}, \qquad (1)$$

where λ is a beam wavelength, $\langle\varepsilon\rangle$ is the microstrain RMS (root-of-mean-square) in the wavevector direction, t_z is the coherent-domain-size (CDS)[9] (the averaged crystallite size, in essence) in the same direction, and θ_{b} is the Bragg scattering angle. The W_{II}^2 vs. ($\tan^2\theta_{\mathrm{b}}$) dependence thus happens to be linear. In measuring the FWHM magnitudes around a series of θ_{b} scattering angles and decomposing them via the Eq. (1), one can thus appreciate two structure parameters of the studied sample, $\langle\varepsilon\rangle$ and t_z.

The temperature annealing in an air atmosphere was performed in a Snol 4/1300 muffle furnace.

The selective wet etching technique was applied in studying the crystal structure defects. Two etchants were used:
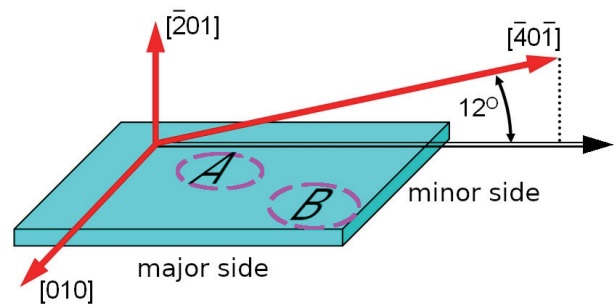

Fig. 1. (Color online) The scheme of the lattice crystallographic basis in the β-Ga$_2$O$_3$ crystal sample. "A region" is the central region with a high level of crystal perfection; "B region" is the edge region with a lower crystal perfection.

KOH and H$_3$PO$_4$, both being widely exploited in the etching of semiconductor crystals, including β-Ga$_2$O$_3$[10−15]. The concentration of H$_3$PO$_4$ was (85% wt.), the concentration of KOH was (45% wt.).

Observation of the etched samples surface relief and determination of the etch pits concentrations were processed using a Nikon Eclipse E200 optical microscope and a Supra 55VP scanning electron microscope (SEM) operating in the secondary electron mode (SE).

All the experiments were performed under normal atmospheric conditions (NTP) and a humidity of 40% RH.

3. Results and discussion

Fig. 1 illustrates the lattice arrangement in a planar cutout sample in a shape of a rectangular parallelepiped. The [−201] direction coincides with the surface normal as it was defined. It was detected that the major side surface of the sample had the normal along the [010] direction. However, since the β-Ga$_2$O$_3$ lattice is monoclinic, the third sample face cannot correspond to any crystallographic plane. The [010] zone directions closest to the physical slice (among the directions with comparably low indices) are [201] (angular distortion 3 deg from the 3rd face normal), [602] (6 deg), [403] (12 deg), [401] (12 deg) and opposite direction [$\bar{4}$0$\bar{1}$]. The [$\bar{4}$0$\bar{1}$] direction (see Fig. 1) projection onto the ($\bar{2}$01) plane (the empty arrow) is not a crystallographic direction. The [$\bar{4}$0$\bar{1}$] vector itself does not belong to the ($\bar{2}$01) plane being deviated from it by about 12 deg.

β-Ga$_2$O$_3$ samples cut from the wafers may vary by crystal perfection in their different regions. It is expected that the highest crystal perfection of the samples will be kept in their central regions, away from the edges. Obviously, the latter will have a reduced crystallinity degree due to the mechanical impact of the cutting process. The XRD studies of both regions in the center (marked as "A region") and near the edge (marked as "B region") of the samples were performed (see Fig. 1).

XRD curves registered in the θ–2θ mode within the 2θ angles range from 10 up to 150 deg for the as-cut β-Ga$_2$O$_3$ samples demonstrate reflections for the β-Ga$_2$O$_3$ lattice only (ICDD database entries #01-074-1776, #00-041-1103) at the angles corresponding to the $\bar{2}$01 and fold reflections up to the $\bar{1}$005 one. The entire XRD curve thus corresponds to a beta gallium oxide single crystal with the plane close to the ($\bar{2}$01) one with the accuracy of about 1−2 arcmin or higher.
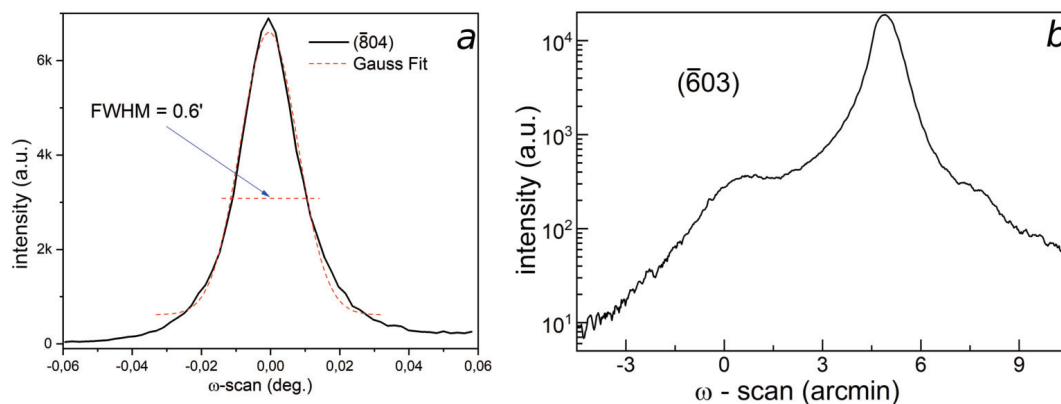
Fig. 2. (Color online) XRD ω-scan curves for the β-Ga₂O₃ in the as-cut sample, (a) 8̄04 reflection of A region; (b) 6̄03 reflection of B region.
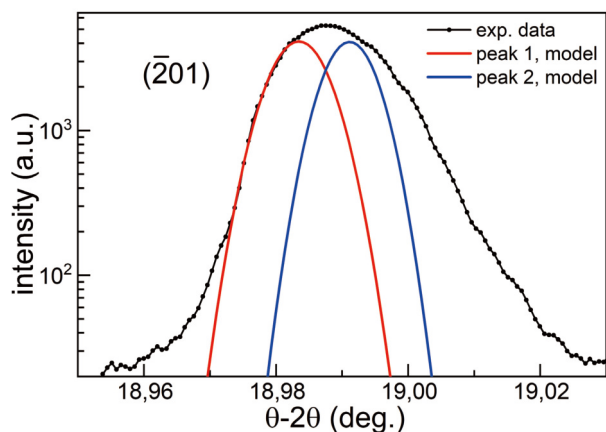

Fig. 3. (Color online) XRD θ−2θ curve pattern for the β-Ga₂O₃ sample in the as-cut state, the 2̄01 reflection, B region.

A set of ω-scanning curves were obtained for the as-cut β-Ga₂O₃ sample for the 2̄01 reflection and fold ones up to 1̄005 for both sample regions (see Fig. 1, A region and B region). The FWHM values of various ω-scan curves registered in the A region happened to be from 30 up to 80 arcsec. Particularly, the 8̄04 peak with the FWHM about 35 arcsec is shown in Fig. 2(a). A high perfection level of the studied sample in its center part can be confirmed hence. In the contrast to that, the FWHM value (~1 arcmin) of the ω-scan registered in the B region displays (see Fig. 2(b)) low crystal perfection. The latter diffraction curve shows the presence of the phase where domains have [2̄01] direction deviation. This indicates the existence of a block fraction with a lattice orientation deviated at an angle of 5 arcmin relative to a major portion of mosaic domains.

In Fig. 3, the θ−2θ curve for the as-cut β-Ga₂O₃ sample registered in the B region is displayed. The peak consists of two separate components that describe reflections corresponding to phases with slightly different lattice parameters. Such peak splitting can be explained by assuming the sample to contain another phase with the deviation of the interplanar distance toward the [2̄01] direction by a fraction of approximately $(1.0-1.5) \times 10^{-4}$ vs. the main plane orientation. Also, the shape of the broadened peak indicates the sample to contain the possible non-stoichiometric phase. Since monoclinic Ga₂O₃ is a stable polymorph, this phase must differ from the dominating one in chemical composition. Approximation of the curves describing the reflections separately is shown in

this figure as red and blue curves without dots. An experimental curve containing two such components holds a strongly distorted shape with a flattened upper part, which does not allow one to perform an united fitting procedure on the base of standard approaches.

At the next step the structural defects of the samples were studied by a selective wet etching technique. This procedure requires a low surface roughness. The roughness parameters were measured with a help of the profilometer. The average roughness and "ten-point-height-of-irregularities" roughness of the surface, detected by a profilometer, had the values of $R_a = 8$ nm, $R_z = 55$ nm, correspondingly. Since this surface was subjected to CMP to produce epi-ready wafer, both roughness values happened to be low as it had been expected. Based on this, the surface was proven to be suitable for the selective wet etching procedure.

Selective wet etching was performed using the following modes: (EM2) 10 min @ 250 °C in H₃PO₄; (EM3) 5 min @ 200 °C in KOH. The choice of etching modes for gallium oxide substrates, utilizing both orthophosphoric acid and potassium hydroxide alkaline is justified in our previous paper[16], where an etching procedure was applied to commercial (2̄01) Ga₂O₃ substrates. Fig. 4 shows SEM images of the sample surfaces (A region) that were subjected to the EM2 and EM3 etching modes (Figs. 4(a) and 4(b), correspondingly). In Fig. 4(a), the elongated etch pits with sizes of the order-of-magnitude of (20×10) μm (major x minor axis) are displayed. They have the common orientation and the average concentration of 2×10^4 cm⁻². The similar etch pits were found (upon etching by the same EM2 mode) in Ref. [16] and denote as x-type etch pits. The etch pits depicted in Fig. 4(b) have smaller sizes, approx. (20×10) μm (major x minor axis). They were also received upon the same EM3 etching mode as in Ref. [16] and named as y-type etch pits. The density of these etch pits has the same value as they appeared in the EM2 mode $(2 \times 10^4$ cm⁻²) in this paper, which satisfy the former results. The orientations of the major axis of both types of etch pits are coinciding with the [4̄01̄] projection direction and the same as in Ref. [16]. Thus, we come to the same conclusion: both types of etch pits considered in this paper have the same origin.

Next, the (2̄01) sample surface near the cutting edge (B region) was analyzed with the help of optical microscopy. All the etching modes revealed an increased etch pit concentration in these areas, but the latter decreasing from the sam-
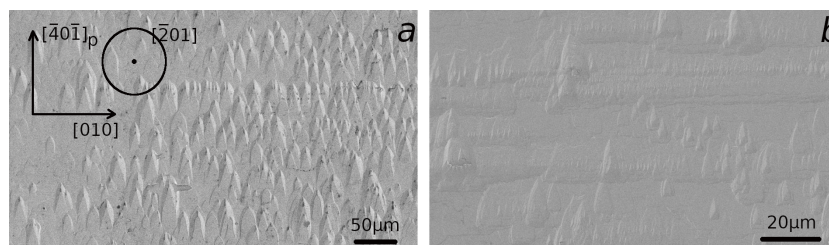
Fig. 4. SEM images of the surface of β-Ga$_2$O$_3$ samples (A region) that were subjected to etching at the following modes: (a) 10 min/250 °C/H$_3$PO$_4$ (EM2); (b) 5 min/200 °C/KOH (EM3). The crystallographic orientation depicted in (a) is applicable for (b). $[\overline{4}0\overline{1}]_p$ is a projection of $[\overline{4}0\overline{1}]$ direction on $(\overline{2}01)$ plane.
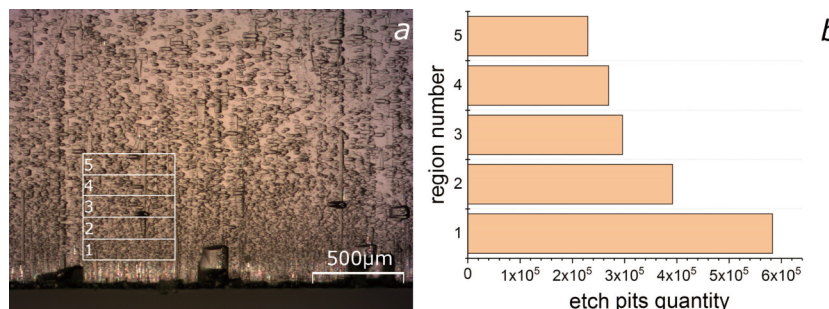

Fig. 5. (Color online) The etching pits distribution along the sample surface (B region): (a) optical image of the surface of the β-Ga$_2$O$_3$ sample subjected to EM2; (b) distribution of the etch pits at this surface.

ple edge to its center (Fig. 5(a), EM2). The pit densities in the selected sectors (1−5) (Fig. 5(a)), which are located along the distance from the cutting line to the center of the sample, were determined and the dependence was plotted (Fig. 5(b)). As it can be seen from Fig. 5(a), already after 500 μm the density value decreases approximately 3 times, the fact illustrating that the structure defect density in the areas subjected to cutting is several times higher than the one of the sample bulk. It should be noted that in the surface region located between the sector 1 and the edge of the sample, the concentration of the etch pits was not determined due to technical difficulties. But it is easy to see (Fig. 5(a)) that in this area the pit concentration is significantly higher. In order to consider the variety of density of etch pits in different sample regions, the values were calculated over its entire area. Thus, such etch pit density (9×10^8 cm^{-2}) should be taken as an average value for the as-cut samples.

In some surface regions of the samples subjected to the EM3 (Fig. 4(b)), besides separate etch pits, a few linear arrays of etch pits aligned along the [010] direction were observed. Similar ordered arrays aligned along the [010] direction were previously obtained in Ref. [17]. The authors proposed that each pit corresponds to a group of edge dislocations that line up to form a small-angle boundary. However, based on the TEM experiment, they abandoned this model and approved another one, according to which these arrays of etch pits display ordered groups of edge dislocations, with a possible slip plane (101). Thus, it should be clarified.

The single crystal subjected to mechanical treatment can split into separate domains divided by domain walls[3], then this crystal becomes a mosaic structure. Initially the crystal structure of a substrate owns residual stresses due to the post-growth treatment[4]. Dislocations distributed in the sub-surface layer being defects of a regular structure create stress fields in the occupied volumes and, as a consequence, have

energetically disadvantageous positions. In the case when dislocations acquire sufficient energy to be mobilized, they tend to move to more favorable locations. They line up in dislocation walls and divide the single crystal onto the block structure. Thus, polygonization occurs, which leads to the appearance of small angle boundaries. Dislocation density over the entire sample decreases, and the migrated dislocations accumulate in the interdomain boundaries. Such process can be displayed as the appearance of etch pit linear arrays. Temperature annealing can activate the dislocation mobilization process. On the other hand, annealing is a technique employed to semiconductor materials to reduce their structural defect density and increase their crystal perfection.

Annealing procedures of the samples were performed in four sequent modes: 1 h@1100 °C = AM1, 3 h@1100 °C = AM2, 5 h@1100 °C = AM3 and 11 h@1100 °C = AM4 (the same sample was used in the certain series, the time value is cumulative). After each annealing step the sample was subjected to selective wet etching in the acid (EM2 etching mode) or the alkali (EM3 etching mode) with the purpose of exploring etch pits. The results registered in the B region are shown (selectively) in Fig. 6: (a) the as-cut sample, (b) AM1 + EM2, (c) AM2 + EM2, (d) AM3 + EM2, (e) AM4 + EM2. In the case of alkaline etching only two steps are displayed: (f) AM3 + EM3 and (g) AM4 + EM3.

The AM1 (Fig. 6(b)) does not lead to significant changes in the sample relief, unless any standalone etch pits appear. SEM images of two next steps AM2 and AM3 (Figs. 6(c) and 6(d), correspondingly) show a large number of etch pits, many of which are aligned. It should be noted that linear arrays, as before, are located along the [010] direction, but in comparison to Fig. 4(b) they have a longer duration, better ordering and a significantly higher density of etch pits. At the same time, the density of separate etch pits has decreased, and they are no longer observed in some regions of the sur-
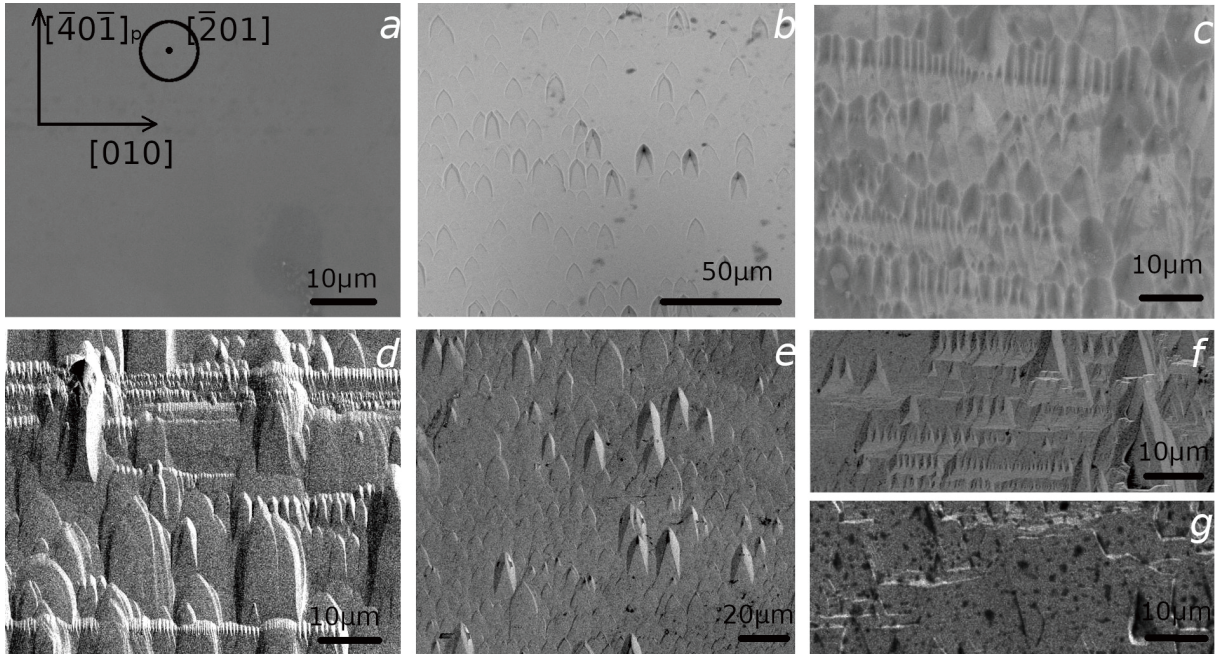
Fig. 6. SEM images of the β-Ga$_2$O$_3$ sample surfaces (B region), subjected to: (a) as-cut sample; (b) AM1 + EM2; (c) AM2 + EM2; (d) AM3 + EM2; (e) AM4 + EM2; (f) AM3 + EM3; and (g) AM4 + EM3. The crystallographic orientation depicted in (a) is applicable for (b−g). $[\bar{4}0\bar{1}]_p$ is a projection of the $[\bar{4}0\bar{1}]$ direction.
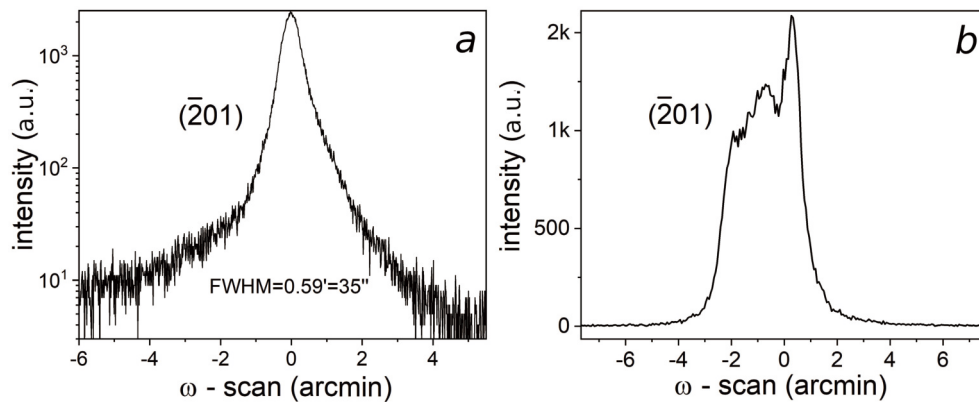

Fig. 7. XRD ω-scan curve for the β-Ga$_2$O$_3$ sample upon the AM2 + EM2 procedure for the $\bar{2}01$ reflection: (a) A region; (b) B region.

face. An average etch pits density calculated for this step has a value of 1×10^7 cm^{-2}. It should be concluded, that, due to temperature annealing, the etch pit density significantly dropped down and the defects of the structure have been redistributed topologically. The latter have concentrated in more energetically favorable regions forming the dislocation walls. On using the AM4 (Fig. 6(e)) procedure, the surface relief changed again: linear arrays of etch pits are not observed anymore, all the pits are distributed homogeneously. The average value of the etch pits density for this step is 8×10^6 cm^{-2} and is the lowest one obtained in this study. Two last annealing steps coupled with alkaline etching are illustrated in Figs. 6(f) and 6(g). The images analysis proves the same tendency as observed in the case of acid etching.

Such a situation (AM4 with corresponding etching procedures) happened at the last step of the process might occur when extended annealing and additional etching destroy the subsurface layer structure or the subsurface layer itself. Although the direct decomposition of trivalent gallium oxide starts at 1200 °C[2], continuous annealing in an atmosphere

not enriched with O$_2$ already at 1100 °C contributes to this process. The processes of lower oxide formation and matter sublimation as well as final etching result in destruction and the removal of the subsurface layer. Defects resulting from post-growth processing and cutting procedure mainly exist in this layer. At this stage of heat treatment linear arrays of etch pits may not occur due to the fact that the basis of the defect structure of deeper layers of the sample is formed mainly by the growth defects. The latter ones are more stable and less mobile then mechanical-originated defects since they were formed under conditions closer to equilibrium ones.

To confirm the hypothesis of dislocation wall formation after the AM2 + EM2 step and the destruction of the subsurface layer structure after the AM4 + EM2 step, an XRD study was carried out.

The ω-scan diffraction curve of the AM2 + EM2 step, registered in the B region displays the presence of the domains with an orientation deviated at 1−3 arcmin for the $[\bar{2}01]$ direction from the position of the dominating set of domains (see Fig. 7(b)). This peak is multiple in contrast to the ω-scan registered in the A region, which, in turn, has a Gauss-like shape
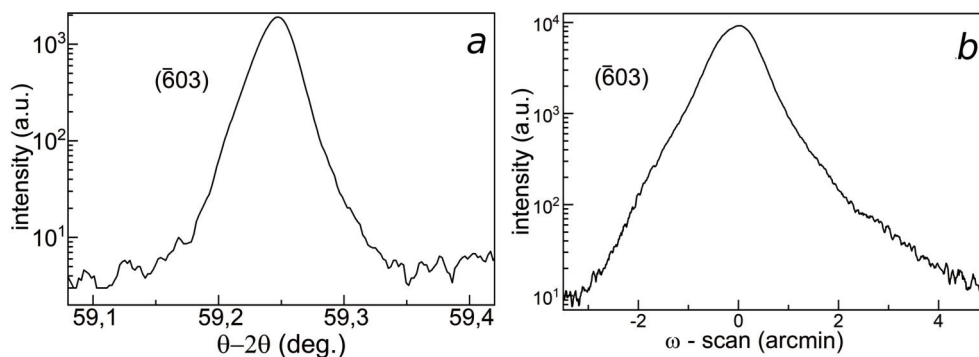
Fig. 8. XRD data for the β-Ga$_2$O$_3$ sample upon AM4 + EM2: (a) θ−2θ curve pattern ($\bar{6}$03 reflection); (b) ω-scan pattern ($\bar{6}$03 reflection); both are registered in the B region.

and a high FWHM value of 35 arcsec (see Fig. 7(a)). Since there is no splitting for any θ−2θ curves, except for those registered for the as-cut samples, there are no phases with changed crystalline parameters, and, consequently, crystal structure of non-stoichiometric composition does not exist within the samples. Thus, vanishing of the non-stoichiometric phase can be associated with etch pit alignment appearance, since they occur simultaneously. One could note that the applied annealing/etching procedures can lead to the removal of layers with a non-stoichiometric composition from the sample.

As long as the θ−2θ curves of the annealed/etched samples registered in the B region demonstrates no reflection splitting, they have a standard shape typical for θ−2θ XRD peaks (i.e., see the θ−2θ curve of the $\bar{6}$03 reflection for the last step procedure (AM4 + EM2) at Fig. 8(a)). This fact allows one to apply standard fitting approaches (based on Gauss, Lorentz, Voigt, etc. functions) and effectively approximate these curves in the range of their dropping down to two orders of magnitude below the maximum. i.e., the XRD dataset describes only a usual isolated reflection here (rather than two or more overlapping reflections which would form a joint peak with a distorted shape incapable of being fitted by standard peak functions). Consequently, there has thus been no more any substantial part of domains with lattice parameters deviation.

In Fig. 8(b), the ω-scan curve for the reflection measured from the sample upon the AM4 + EM2 step in the B region is depicted. As it can be seen in the figure, the ω-curve has a standard Gauss-like shape. It can be concluded hence that the curve is not influenced by any valuable fraction of domains with orientation deviated in the [$\bar{2}$01] direction vs. the dominating phase. It has been confirmed once more that the annealing/etching processes of the sample treatment managed to minimize the block disorientation within the sample matter. At the same time the surface relief also changes, losing etch pit alignment.

The behavior of XRD peaks measured for as-cut samples and ones after AM2 + EM2 and AM4 + EM2 steps etching procedures is illustrated in the Table 1. All of them are registered in the B region. In each case, it represents the angles between the dominating peak and its most intensive neighbors. As it was written earlier, such angles describe the orientation deviation at ω-scanning curves. In the case of θ−2θ curves, such angles are responsible for the change in the lattice parameters and, hence, non-stoichiometric composi-

Table 1. XRD measurements for the β-Ga$_2$O$_3$ sample, the B region. Average peak splitting for curves of diffraction reflection (CDR) related to the stage of measuring, the CDR type (θ−2θ or ω-scanning), and the reflection set-of-indices.

| CDR | Extra peak shift (arcmin) | | | | | |
| | As-cut | | AM2 + EM2 | | AM4 + EM2 | |
	θ−2θ	ω	θ−2θ	ω	θ−2θ	ω
$\bar{2}$01	0.5	−0.6, 0.7	0	−0.8	0	1.1
$\bar{4}$02	1.5	±0.7	0	0.7	0	0
$\bar{6}$03	0	−1.0, 0.8	0	0.7	0	0
$\bar{8}$04	0	0	0	1.0	0	0
$\overline{10}$05	0	−2.7, 2.9	0	1.8	0	0

tion for some sample fraction. As it can be concluded from Table 1, in the as-cut state, both spatially deviated and non-stoichiometric fractions used to exist simultaneously. Domains deviated in orientation by 0.6−1.0 arcmin as well as about 3 arcmin in two opposite directions close to ±[010] were observed. Then, after the AM2 + EM2 treatment, any non-stoichiometric phases disappeared or carried out to be unperceivable. Finally, on applying the AM4 + EM2 procedure, the phases with deviated orientation also seemed to have vanished. The ω-scanning curves no longer contain deviated peaks of substantial intensity with an exception of the $\bar{2}$01 one where a strongly expanded sample region is affected due to the low incident angle. As to θ−2θ reflection functions, they were not split at both AM2 + EM2 and AM4 + EM2 stages, though in the as-cut state there were extra peaks corresponding to the lattice size relative discrepancy $(1.0−1.5) \times 10^{-4}$ in the [$\bar{2}$01] direction.

Besides, the Williamson−Hall model was applied to the θ−2θ curves for the samples in the B region at all the stages of annealing/etching procedures. This approach made it possible to reveal the dynamics of changes in lattice parameters in different regions of the β-Ga$_2$O$_3$ samples. A preliminary estimation of all the processed θ−2θ curves shape without taking into account the hardware function showed that at all stages of the sample treatment, the CDS values are in the range of 400−600 nm. This is the lowest limit of the sample domain size in the [$\bar{2}$01] direction. Thus, domains remain almost unchanged in size, but are getting closer in orientation with annealing time increasement.

It also can be concluded that the formation of small angle boundaries appeared mainly due to the involvement of defects originated by cutting procedure, because of their

high mobility. After their annihilation due to the removal of the upper part of the sample subsurface layer, most of the defects remaining are growth ones, which have less mobility, hence their transformation and formation of groups impedes.

Jointly with the results of XRD curves study, $\theta-2\theta$ curves processing and analyzing etch pits density and distribution, one can conclude that the applied annealing/etching procedures led to decrease defect density and enhanced crystal perfection.

4. Conclusions

The structure of near-edge regions of the samples, which were cut from the epi-ready ($\bar{2}$01) β-Ga$_2$O$_3$ wafer, consists of separate blocks and has high defect density. There are blocks with misorientation at angles of 1−3 arcmin relative to a major portion of mosaic and discrepancy between the lattice sizes of about $(1.0-1.5) \times 10^{-4}$ in the [$\bar{2}$01] direction. $\theta-2\theta$ curve peak splitting indicates the presence of a non-stoichiometric extra phase in the sample. The defect density, estimated from the average etch pits value, calculated over the entire sample surface including near-edge regions, was about 9×10^8 cm^{-2} initially and then reduced by high temperature annealing. The etching of annealed samples within 3 h at 1100 °C reveals linear arrays aligned along the [010] direction, which are associated with small-angle dislocation boundaries. The disappearance of the $\theta-2\theta$ curve peak splitting is accompanied with the elimination of fractions with the lattice size relative discrepancy and the removal of the non-stoichiometric phase. Increasing annealing duration up to 11 h coupled with etching liquidates the linear arrays and distributes etch pits homogenously. The applied procedure in the total resulted in a significant decrease in average density of the etch pit value to 8×10^6 cm^{-2}. The fractions with spatial orientation deviation of 1−3 arcmin are shown to exist both in the as-cut samples and after the 3 h annealing, becoming unperceivable after 11 h one. Approaching the ω-scan peak in annealed samples to the Gauss-like one shows an improvement in their crystal quality.

Acknowledgments

References

[1] Pearton S J, Yang J C, Cary P H IV, et al. A review of Ga$_2$O$_3$ materials, processing, and devices. Appl Phys Rev, 2018, 5, 011301

[2] Stepanov S I, Nikolaev V I, Bougrov V E, et al. Gallium oxide: properties and applications− a review. Rev Adv Mater Sci, 2016, 44, 63

[3] Butenko P N, Guzilova L I, Chikiryaka A V, et al. Impact on the subsurface layers of the single-crystal β-Ga$_2$O$_3$ wafers induced by a mechanical wear. Mater Sci Semicond Process, 2022, 143, 106520

[4] Gao S, Wu Y Q, Kang R K, et al. Nanogrinding induced surface and deformation mechanism of single crystal β-Ga$_2$O$_3$. Mater Sci Semicond Process, 2018, 79, 165

[5] Huang C J, Mu W X, Zhou H, et al. Effect of OH$^-$ on chemical mechanical polishing of β-Ga$_2$O$_3$ (100) substrate using an alkaline slurry. RSC Adv, 2018, 8, 6544

[6] Oshima T, Hashiguchi A, Moribayashi T, et al. Electrical properties of Schottky barrier diodes fabricated on (001) β-Ga$_2$O$_3$ substrates with crystal defects. Jpn J Appl Phys, 2017, 56, 086501

[7] Kasu M, Oshima T, Hanada K, et al. Crystal defects observed by the etch-pit method and their effects on Schottky-barrier-diode characteristics on (-201) β-Ga$_2$O$_3$. Jpn J Appl Phys, 2017, 56, 091101

[8] Williamson G K, Hall W H. X-ray line broadening from filed aluminium and wolfram. Acta Metall, 1953, 1, 22

[9] Boiko M E, Sharkov M D, Boiko A M, et al. Investigation of the atomic, crystal, and domain structures of materials based on X-ray diffraction and absorption data: A review. Tech Phys, 2015, 60, 1575

[10] Yao Y Z, Sugawara Y, Ishikawa Y. Observation of dislocations in β-Ga$_2$O$_3$ single-crystal substrates by synchrotron X-ray topography, chemical etching, and transmission electron microscopy. Jpn J Appl Phys, 2020, 59, 045502

[11] Yao Y Z, Sugawara Y, Sato K, et al. Etch pit formation on β-Ga$_2$O$_3$ by molten KOH+NaOH and hot H$_3$PO$_4$ and their correlation with dislocations. J Alloys Compd, 2022, 910, 164788

[12] Lu D Z, Jiang Q T, Ma X M, et al. Defect-related etch pits on crystals and their utilization. Crystals, 2022, 12, 1549

[13] Mazzolini P, Vogt P, Schewski R, et al. Faceting and metal-exchange catalysis in (010) β-Ga$_2$O$_3$ thin films homoepitaxially grown by plasma-assisted molecular beam epitaxy. APL Mater, 2019, 7, 022511

[14] Huang H C, Ren Z J, Chan C, et al. Wet etch, dry etch, and MacEtch of β-Ga$_2$O$_3$: A review of characteristics and mechanism. J Mater Res, 2021, 36, 4756

[15] Ogawa K, Ogawa N, Kosaka R, et al. AFM observation of etch-pit shapes on β-Ga$_2$O$_3$ (001) surface formed by molten alkali etching. Mater Sci Forum, 2020, 1004, 512

[16] Zarichny A A, Butenko P N, Boiko M E, et al. The analysis of the etch pits parameters in the ($\bar{2}$01) plane of the β-Ga$_2$O$_3$ substrate crystals. Materials Physics and Mechanics, 2023, 51(3), 174

[17] Ueda O, Ikenaga N, Koshi K, et al. Structural evaluation of defects in β-Ga$_2$O$_3$ single crystals grown by edge-defined film-fed growth process. Jpn J Appl Phys, 2016, 55, 1202BD

Pavel Butenko received his PhD from Peter the Great St. Petersburg Polytechnic University, St. Petersburg, Russia in 2006. He has held various positions at universities in Russia, Germany and China. He is currently a senior researcher in Physics of Shaped Crystals Laboratory, Solid State Physics Department at Ioffe Institute, Russian Academy of Sciences, St. Petersburg, Russia and Laboratory of Ultrawide Bandgap Semiconductors, Department of Semiconductor Electronics and Semiconductor Physics at MISIS University, Moscow, Russia. His research interests include: metal-oxide semiconductors; liquid-phase crystal growth and epitaxy; obtaining free-standing substrates by exfoliation; structure characterization; structure defects.

Michael Boiko received his PhD in Ioffe Institute, Russian Academy of Sciences, Saint-Petersburg, Russia in 1993. He is currently associated professor with Ioffe Institute. At present his research interest include XRD, SAXS, EXAFS of crystal structure and super structure of domains in semiconductors and dielectrics.
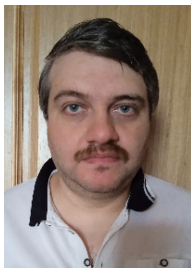
Mikhail Sharkov received his PhD in Ioffe Institute, Russian Academy of Sciences, St. Petersburg, Russia in 2009. Now he is working in the same institute at a position of senior researcher. His regions of interest are X-ray-based methods of materials studying, semiconductor heterostructures and XRD data modeling.

Vladimir Krymov received his PhD in Ioffe Institute, Russian Academy of Sciences, St. Petersburg, Russia in 1978. No he is working as a senior researcher at the Ioffe Institute, Russian Academy of Sciences. His research interests include the growth and characterization of sapphire and gallium oxide bulk crystals.

Aleksei Almaev received his PhD in the area of Physical and Mathematical Sciences from National Research Tomsk State University, Tomsk, Russia, in 2018. He is currently a Head of the Laboratory of Metal Oxide Semiconductors at Research and Development Center for Advanced Technologies in Microelectronics of the National Research Tomsk State University. His current research interests are metal oxide semiconductors, related devices and functional coatings.
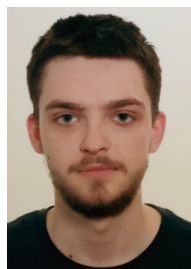
Anton Zarichny got his bachelor's degree in 2017 and his master's degree in 2023 from Peter the Great St. Petersburg Polytechnic University, St. Petersburg, Russia. Now he is a PhD student in Physics of Shaped Crystals Laboratory at Ioffe Institute, Russian Academy of Sciences. His research focuses on the characterization of ultrawide bandgap metal-oxide semiconductors.

Aleksnder Kitsay received his Master's degree in engineering in 1976 from St. Petersburg State Institute of Technology, St. Petersburg, Russia. He worked as a researcher at the V. G. Khlopin Radium Institute, St. Petersburg, Russia. He is currently a researcher in Physics of Shaped Crystals Laboratory, Solid State Physics Department at Ioffe Institute, Russian Academy of Sciences. His current research interests include semiconductor crystal growth by flux method.

Vladimir Nikolaev received a PhD in solid state physics from the Ioffe Institute, St. Petersburg, Russia in 1989. In 1990, Dr. Nikolaev was awarded the Prize of the Physical Society of the Ioffe Institute for the discovery of the electro-plastic effect in ferroelectric crystals. Currently, Dr. Nikolaev is the Head of the Physics of Shaped Crystals laboratory at the Ioffe Institute. He is also the founder and CEO of Perfect Crystals LLC. He has published more than 300 scientific articles in peer-reviewed journals, has six granted patents and several chapters in books on electronics and smart materials. He is on the editorial board of the *Technical Physics* journal.